



## Thermal Effect of Cooling the Cathode Grid Tabs of a Lithium-Ion Pouch Cell

Stephen J. Bazinski\* and Xia Wang\*\*,<sup>z</sup>

Department of Mechanical Engineering, Oakland University, Rochester, Michigan 48309, USA

Infrared thermography shows that the joint between the cathode grid stack and the cell tab is a source of Joule heating within a lithium-ion pouch cell. This can exacerbate thermal gradients within the cell core if the C-rate is sufficiently high. This paper studies the heat generated at the cathode tab joint of a 14Ah lithium iron phosphate (LFP) pouch cell. The heat generation was quantified by using an energy balance equation and the average heat transfer coefficient was calculated by modeling the cell as an isothermal vertical plate in natural convection. The influence of this heat on the cell's thermal gradients was studied during a 3C and 8C rate of discharge. It has been found that removal of this heat at its source can appreciably lower the overall average surface temperature of the cell. However, at a 3C rate discharge, the removal of this heat can induce a greater thermal gradient within the cell core. At an 8C rate of discharge, there is a minimal improvement in the temperature gradient. As a result, a thermal management system which incorporates cathode tab heat removal would most likely be an ineffective design feature.

© The Author(s) 2014. Published by ECS. This is an open access article distributed under the terms of the Creative Commons Attribution Non-Commercial No Derivatives 4.0 License (CC BY-NC-ND, <http://creativecommons.org/licenses/by-nc-nd/4.0/>), which permits non-commercial reuse, distribution, and reproduction in any medium, provided the original work is not changed in any way and is properly cited. For permission for commercial reuse, please email: [oa@electrochem.org](mailto:oa@electrochem.org). [DOI: 10.1149/2.0731414jes] All rights reserved.

Manuscript submitted July 31, 2014; revised manuscript received October 6, 2014. Published October 16, 2014. This was Paper 111 presented at the Toronto, Canada, Meeting of the Society, May 12-16, 2013.

Maintaining uniformity of temperature between cells is an important factor in the thermal management of lithium-ion batteries. It is desirable for this variation to be in a tight range.<sup>1</sup> Rugh et al. stated that temperature gradients should be kept to less than 3°C to 4°C throughout the battery pack.<sup>2</sup> Failure to meet this criterion has a direct effect on decreasing the battery pack life. In addition, they also advocate an operating temperature range of 15°C to 35°C for the pack. Excursions beyond this range have repercussions as well. It has been found that the lifespan for a lithium-ion cell is reduced by approximately 2 months for every degree of temperature rise while operating in a temperature range of 30°C to 40°C.<sup>3</sup> Capacity and power degradation is also accelerated at elevated temperatures.<sup>4-9</sup>

The lithium iron phosphate (LFP) cell chemistry is gaining wide acceptance in electric vehicle applications.<sup>10</sup> Its inherent ability to tolerate abusive conditions and resist thermal runaway is especially attractive to battery pack designers. Battery manufacturers have responded by offering high capacity cells in a pouch format. This format affords better packaging efficiency and offers a very favorable area-to-volume ratio to facilitate thermal management. As a result, this work uses a high capacity LFP pouch cell.

The temperature near the cathode terminal of a pouch cell is consistently higher than that at the anode, due to differences in the thermal conductivities of the metals used as current collectors. This is true regardless of the particular lithium-based electrochemistry being used. The higher electrical resistivity of the aluminum used in the positive electrode as compared to the copper negative electrode (about 37%) creates a greater source of Joule heating between the two. An additional factor is the thermal contact resistance that comes from the joining process of the grid tab stack. Typically, ultrasonic metal welding of the grid tabs is performed during the assembly of the cell core.<sup>11</sup> This manufacturing process may result in localized microscopic gaps between mating tabs in the stack and decrease the effective area for current flow. There are other joining methods available (e.g. resistance spot welding and laser beam welding) but the materials and tab joint design often cannot meet the process requirements.<sup>12</sup> In some high capacity cells, the tab stack is too thick for ultrasonic welding alone and a secondary operation is needed that involves a riveted bar joint to provide added clamp load. The necessary creation of rivet holes in the grid tab stack only reduces the effective area even more.

The thermal image in Figure 1 shows that the stack joint on the cathode tabs is always the first “hotspot” to appear on the cell face during either a charge or discharge cycle. The same thermal image of the anode side, however, shows that its temperature increases at approximately the same rate as the rest of the cell. Any temperature increase in this area is mainly due to heat transmission from the cathode.

Thermal management of pouch cells on a module level is done by several different methods that can be categorized as being either liquid or air cooled. Direct-liquid cooling with heat exchange plates placed between each pouch cell is one type of design and is used by the Chevrolet Volt. Direct-air cooling of the module is another approach to thermal management in which a fan circulates air around each module and is the one employed by the Nissan Leaf. In the other category, indirect liquid cooling of the module, as the name implies, transfers heat from the cell to the working fluid via conduction through an intermediate component. Phase change materials (PCM) have been investigated for the potential to be used for battery cooling.<sup>13</sup> However, PCMs are not widely used due to the temperature at which the phase change occurs. It can be difficult to find a PCM with an adequate thermal conductivity and the right melting point to be useful in battery cooling under all operating conditions.

The purpose of this study is to quantify the effects on the average temperature and temperature gradients of the cell face due to resistive heating of the cathode tab stack at different rates of discharge. This will help decide whether or not an opportunity exists to design an effective thermal management system that focuses on controlling the heat generated at the cathode grid tab stack.

### Experimental

The research investigated heat generation of a lithium iron-phosphate (LFP) pouch cell from Energy Innovation Group (EiG). This commercially available cell uses a graphite anode and is encased in a laminated aluminum pouch. The cell specifications are listed in Table I. As done in past studies by other researchers, it is assumed that thermal properties are isotropic.<sup>14</sup> The specific heat,  $c_p$ , of the cell was measured by an isothermal calorimeter as a function of temperature. This function was found to be:

$$c_p = 0.0073T_{\text{cell}} + 1.2064 \quad [1]$$

where  $c_p$  is measured in  $\text{Jg}^{-1}\text{°C}^{-1}$  and  $T_{\text{cell}}$  is the average cell temperature ( $\text{°C}$ )

\*Electrochemical Society Student Member.

\*\*Electrochemical Society Active Member.

<sup>z</sup>E-mail: [wang@oakland.edu](mailto:wang@oakland.edu)

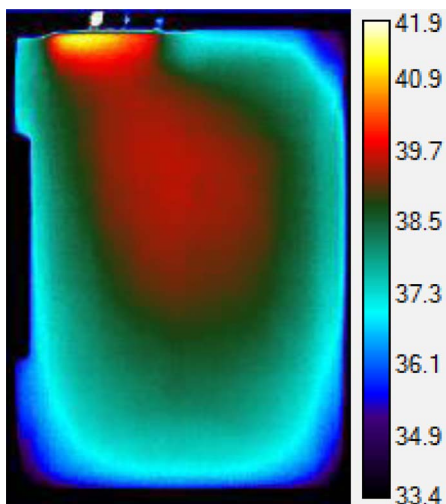


**Figure 1.** Thermal image of a lithium-ion pouch cell discharging at a 5C rate in ambient air. Cathode terminal is in the upper left corner of pouch cell.

The cell was initially at ambient temperature within a draft barrier without ventilation. The cell was fully discharged from 100% State-of-Charge (SOC) at a constant current. It was held in a vertical orientation and underwent natural convection during cycling with the long edge of the pouch parallel to the ground. The temperature of the cell surface was recorded with a FLIR SC325 infrared thermal camera with an accuracy of  $\pm 2^\circ\text{C}$ . Special caution must be taken in order to take the accurate measurement using the infrared camera. For example, the cell was coated with a white boron nitride spray. This was done for two reasons: 1) to meet the minimum emissivity requirements for infrared measurement and 2) to avoid the camera's reflection on the pouch from being recorded by its sensors. This is a crucial step. As the emissivity deviates from the ideal blackbody, the IR camera signal loses its fidelity due to reflective components.<sup>15</sup> As a ceramic spray, the boron nitride crystals create an extremely thin and diffuse layer on the cell face. It is used for this purpose in thermo graphic studies of electrical components by the National Renewable Energy Laboratory (NREL) and Army Research Laboratory.<sup>16</sup> Even though only one cell face is presented to the infrared camera, it was important to ensure that both sides have the same highly matte surface ( $\epsilon = 0.90$ ). As opposed to carbon black or spray-on paints, boron nitride has the advantage of being easily removed with soap and water. The assumption of identical thermal behavior of the cell faces requires this condition. The cell tabs were masked prior to spraying to ensure that they remained clean for electrical connection. A 10-channel Maccor Model 4200 System cycler was used to discharge the cells and acquire data.

Removal of the cathode tab stack heat was accomplished by attaching a cold plate directly to the cell as shown in Figure 2. The CP-25 copper cold plate from Lytron Inc. has a unique gull-wing design for operation in small spaces. Compressed air flowing at a constant 30 SCFM and  $23^\circ\text{C}$  was used as the working fluid. This was due to better



**Figure 2.** Cold plate used to remove heat from the cathode tab stack. Image courtesy of Lytron Inc.

safety and ease of setup as compared to using circulating water. Thin copper foil strips were used as a thermal interface material between the cold plate and the uneven pouch surface adjacent to the cathode grid tab stack. This served to bridge any air gaps and improve heat transfer.

The cell was clamped along its sealed edge by a vise with insulated grippers. The cell was positioned so that the longer side was presented as the leading edge of the boundary layer. This was done to encourage laminar flow by minimizing the characteristic length. The cold plate was held in place against the cathode grid tab stack by spring-loaded hand clamps. Figure 3 shows the front and rear views of the setup. Unfortunately, the discharge current of every test run exceeded the 30A limit of the test channel. As a result, it was necessary to connect the electrical leads from several channels to the tabs. The entire setup was later enclosed by partition walls to block air drafts. Natural convection is a required test condition as the temperature gradient within a cell increases with increased surface convection.<sup>17</sup>

The experimental procedure can be summarized in the steps listed below:

- 1) Fully discharge cell in natural convection at 3C rate of constant current without a cold plate on the cathode grid tab stack. Record data with the infrared camera.
- 2) Record cell surface temperature during 3C discharge from 100% SOC with the air-cooled copper heat exchanger attached on cathode grid tab stack.
- 3) Use the temperature profile to calculate the  $h$  values for each data point.
- 4) Calculate the heat generation within the cell for each test run.
- 5) Determine the resulting heat contribution due to the cathode tab resistance.
- 6) Determine difference in cell thermal gradients between the two setups using FLIR software data analysis.
- 7) Repeat Steps #1 - #6 during an 8C discharge of the cell.

### Theoretical Analysis: Heat Generation

*Determining heat rates.*— There are two types of heat sources within an operating cell: reversible and irreversible. Reversible heat (or entropic heat) can either be exothermic or endothermic in nature depending on the SOC of the cell and the direction of current flow. Irreversible heat is always exothermic and is due to the resistance of the inner components to conduct electron and ion flows. Combined, these resistances constitute Joule heating. A portion of the resistance to electron flow resides in the joint formed between the current grid tabs and the terminals. In short, for a cell that has no cooling plate applied to its cathode tab, this relationship can be stated as:

$$\dot{Q}_{\text{Joule}} = \dot{Q}_{\text{cell core}} + \dot{Q}_{\text{anode tab}} + \dot{Q}_{\text{cathode tab}} \quad [2]$$

The total heat generated within the cell core is the sum of all sources of heat from that assembly (resistive, polarization, and entropic). Cooling the cathode tab would have the effect of removing the last term on the RHS of Eqn. 2. It is assumed that the cathode tab joint resistance is constant between the cooled and uncooled setups for both

**Table I. Cell Specifications.**

Height	220 mm
Width	140 mm
Thickness	7 mm
Mass	385 g
Nominal Capacity	14Ah
Maximum Charge Voltage	3.65 V
Nominal Voltage	3.2V
Minimum Discharge Voltage	2.0V
Maximum Charge Current	1C
Maximum Discharge Current	10C

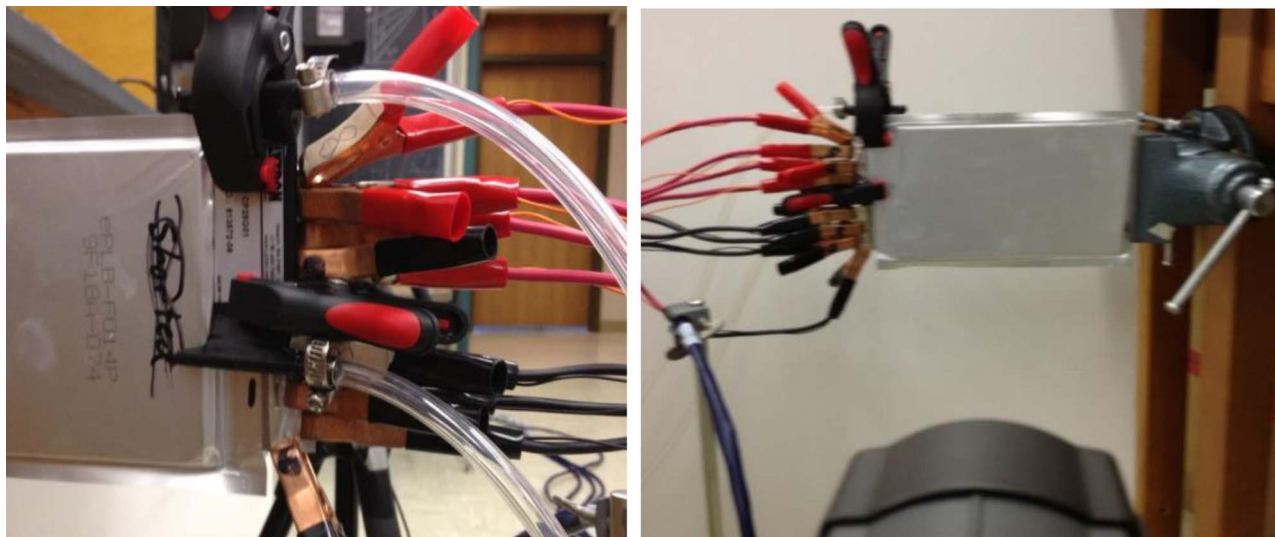


**Figure 3.** Rear view (left image) showing the air hoses and multiple channel use. The front view (right image) of the setup shows the FLIR camera in the bottom.

the 3C and 8C discharges. It is also assumed that the average cell surface temperature is an acceptable measurement for the volumetric temperature. As a result, the task of determining the heat generated under various rates of discharge can now be done with the use of the following energy balance equation:<sup>18</sup>

$$\dot{Q}_{\text{generated}} = mc_p \frac{dT_{\text{cell}}}{dt} + hA(T_{\text{cell}} - T_{\infty}) + \varepsilon\sigma A(T_{\text{cell}}^4 - T_{\infty}^4) + \dot{Q}_{\text{tab}} \quad [3]$$

where,  $m$  is the cell mass (g),  $dT_{\text{cell}}/dt$  is the rate of temperature change of the cell surface as a function of time during discharge,  $h$  is the natural convection coefficient ( $\text{Wm}^{-2}\text{K}^{-1}$ ),  $A$  is the surface area of the cell ( $\text{m}^2$ ), and the last term quantifies the heat loss through tab cooling.  $\dot{Q}_{\text{tab}}$  represents any heat loss that may occur through tab cooling. While there is tab cooling, the quantity of removed heat will result in a lower cell temperature.

*Determining the convection coefficient:  $h$ .*— Obtaining an accurate value for the convection coefficient of a body in a transient state is difficult to do yet it is of the utmost importance. Some analytical approaches, such as the lumped capacitance model, are available that will yield an average composite  $h$  value for an isothermal body undergoing a cooling or heating process. This composite parameter is the total effect of not only natural convection but also of radiation. However, this composite value has two caveats: 1) it assumes no internal heat generation and 2) is considered to be constant throughout the process regardless of the temperature difference between the body and fluid. To apply these conditions to the experimental setup would undoubtedly introduce error into the results.

In order to avoid this error, the cell was treated as a vertical plate in natural convection. Based on measurements of the ambient air conditions and cell face temperature, psychrometric properties were found. These, in turn, were used to calculate dimensionless parameters (e.g. Prandtl, Rayleigh, and Nusselt) which had physical interpretations that related to conditions in the boundary layer. All fluid properties in the boundary layer are evaluated at a temperature that is the average of the cell surface and ambient air. This yielded the average natural convection coefficient of the cell for each temperature data point by using the following formula:

$$h_{\text{avg}} = \overline{\text{Nu}} \frac{k_f}{L} \quad [4]$$

where  $\overline{\text{Nu}}$  is the average Nusselt number and is found by Eqn. 5 for natural convection,<sup>19</sup>  $k_f$  is the thermal conductivity of the boundary layer fluid ( $\text{Wm}^{-1}\text{K}^{-1}$ ), and  $L$  is the characteristic length of the cell

face (0.14 m).

$$\overline{\text{Nu}} = 0.68 + \frac{0.670\text{Ra}^{1/4}}{[1 + (0.492/\text{Pr})^{9/16}]^{4/9}} \quad [5]$$

where  $\text{Ra}$  is Rayleigh number and Prandtl is number, which are determined based on the measured air properties. The Rayleigh number is associated with buoyancy driven flow and is found by the following:

$$\text{Ra}_L = \frac{g\beta}{\nu\alpha} (T_{\text{cell}} - T_{\infty})L^3 \quad [6]$$

where  $g$  is the acceleration due to gravity ( $9.81 \text{ m/sec}^2$ ),  $\beta$  is the thermal expansion coefficient of the fluid ( $\text{K}^{-1}$ ),  $\nu$  is the kinematic viscosity ( $\text{kg}^*\text{m}^{-1}\text{sec}^{-1}$ ), and  $\alpha$  is the thermal diffusivity ( $\text{m}^2/\text{sec}$ ). The Prandtl number is the ratio of the viscous diffusion rate to the thermal diffusion rate of the boundary layer fluid. It is defined by:

$$\text{Pr} = \frac{\nu}{\alpha} \quad [7]$$

These thermodynamic properties were compiled for each temperature data point throughout the discharge in a spreadsheet program developed by the researchers. The spreadsheet formulas were validated by comparing the calculated thermodynamic properties to those yielded by a website that offers a professional-quality psychrometric calculator.<sup>20</sup> This calculator uses real gas formulations developed by Hyland and Wexler and is approved by the American Society of Heating, Refrigeration, and Air Conditioning Engineers (ASHRAE).<sup>21,22</sup>

*Validating the computed convection coefficient.*— The next task was to check the accuracy of the convection coefficient in an experimental setup. A heat calibration cell was used that comprises of two thin aluminum plates to mimic the cell faces and eight Kapton heaters mounted within the assembly to provide a known heat generation. Figure 4 shows the construction of this assembly. With constant heat generation, the assembly was allowed to reach steady-state with its environment while suspended in a vertical orientation. Once this was attained, it can be established that the total heat loss through convection and radiation must be equal to the known heat generation of the heaters. At thermal equilibrium, the rate of heat storage (first term on the RHS of Eqn. 3) becomes zero and it conveniently becomes unnecessary to calculate the specific heat capacity for the calibration cell assembly.

Temperature measurements derived from a snapshot of an infrared image of the calibration cell were analyzed. After inputting the relevant parameters, temperatures, and test conditions into the spreadsheet model, the model predicted the resulting  $h$  value of the calibration

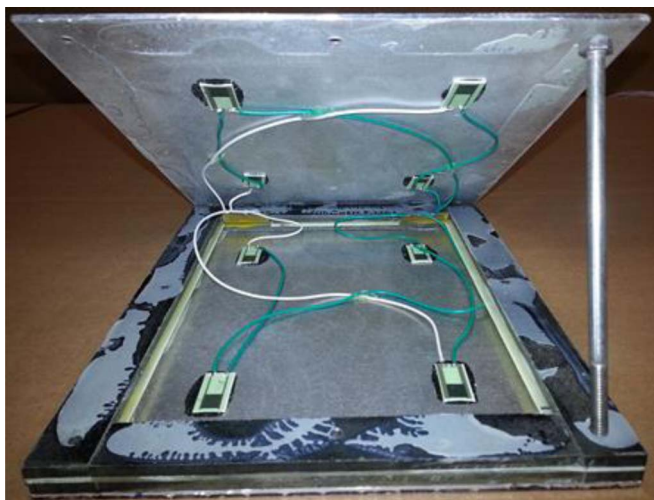


**Figure 4.** Interior view of the calibration cell used to validate the measured convection coefficient. Note the four Kapton heaters mounted on the inner face of each aluminum plate. When assembled, the outside surface of these plates act as the cell faces and provide a known heat output.

cell. This was then inserted into the following classic heat convection equation:

$$\dot{Q}_{\text{conv}} = h_{\text{avg}} A (T_{\text{cell}} - T_{\infty}) \quad [8]$$

When the predicted heat from Eqn. 6 was compared to that produced by the heaters, the values were within 7%. A data plot of the  $h$  values calculated during both the 3C and 8C rates are shown in Figures 5a and 5b respectively.

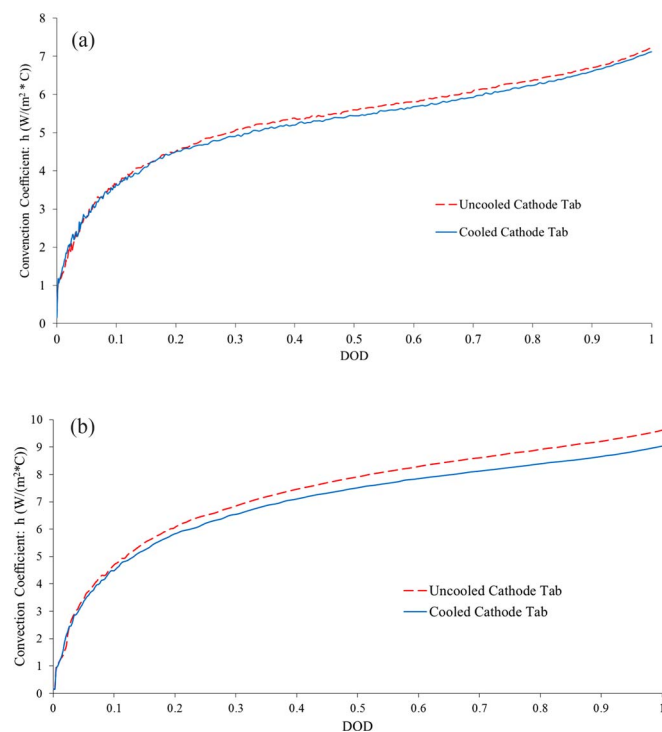


**Figure 5.** (a) Predicted convection coefficient values,  $h$ , for the test cell undergoing a 3C discharge with and without cooling of the cathode tabs. (b) Predicted convection coefficient values,  $h$ , for the test cell undergoing an 8C discharge with and without cooling of the cathode tabs.

*Determining the  $dT_{\text{cell}}/dt$  term.*— The simplicity of equation 3 is detracted by the difficulty in obtaining an accurate and representative value for the  $dT_{\text{cell}}/dt$  term. Random signal noise in the temperature reading of the infrared camera becomes more prevalent in the  $dT_{\text{cell}}/dt$  calculation as the time span approaches zero. This results in a plot of the heat curve with widely varying oscillations. This pitfall was somewhat mitigated by the use of curve-fitting software. As a result, it was possible to replace the fluctuations in the temperature data with a smooth polynomial fit that had a very high correlation to the original curve.

Another drawback to the  $dT_{\text{cell}}/dt$  term is that it characterizes a surface phenomenon while the heat generation is a volumetric phenomenon. There is an unavoidable time lag of the cell surface response to the electrochemical processes occurring within the bulk mass. This disparity becomes greater at higher C-rates due, in large part, to the relatively low thermal conductivity of the cell along its thickness.

## Results and Discussion

One feature of the FLIR software is the ability of the user to designate a Region of Interest (ROI). By creating and positioning a ROI on the thermal image, the user can have the software perform a variety of statistical analyses on only those pixels that are contained within it. In this study, a rectangular ROI was positioned to encompass the cell pouch perimeter. This allowed temperature data to be analyzed not only for the entire cell face but its exact center point as well. No attempt was made to ascertain the core temperature of the cell during testing. Thermography is only capable of measuring surface phenomena. However, this particular pouch cell is thermally thin and it is assumed that it can be treated as a lumped mass. The frame frequency for the FLIR camera was 9 Hz.

*Results: 3C discharge.*— In Figure 6a, the average overall surface temperature is lowered by less than 1°C due to cathode cooling. As shown in Figure 6b, the temperature at the center of the cell face was nearly unaffected by the removal of cathode tab heat. This indicates that the driving force was almost too weak for the heat to conduct to the cell face center throughout the entire discharge. Figure 7 shows thermal images of the cell at the end of a 3C discharge with and without cathode tab cooling.

At a 3C discharge, cooling the cathode tab stack has a minimal effect in the overall heat generation. Figure 8 shows the calculated heat rates within the cell core being relatively close with each other. On average, the cell with a cooled cathode tab had a heat rate that was approximately 1.05W lower than that of the uncooled cell (8.74W vs. 9.79W respectively).

*Results: 8C discharge.*— Figure 9a summarizes the average surface temperature data for the 8C discharge rate. Here, the average cell surface temperature was 5°C higher (52.5°C vs. 47.5°C) due to the presence of cathode tab heat. Note from Fig. 9b that the heat from the cathode grid tab stack influences the average cell temperature and the center of the cell surface after approximately 11% DOD. It appears that the benefits of lower cell temperatures due to the cooling the cathode grid tab stack are only evident at high rates of discharge.

By applying Eqn. 3 to the data, heat generation within the cell core throughout the discharge was calculated for each trial run. The results are presented in Figure 10. The average difference between the two heat rates is approximately 6.75W (47.93W for the uncooled vs. 41.18W for cooled).

*Validating the calculated heat from the cathode tab.*— In theory, the cathode tab heat should have a ratio of 7.11 between the 8C and 3C discharges ( $8^2/3^2$ ) since the Joule heating varies as the square of the current flow. The empirical data shows this ratio to be (6.75W/1.05W) or 6.43. This is within 10% of the theoretical value and is, therefore, in good agreement. This ratio is based on the assumption that the heat generation within the core assembly is the same regardless of whether the cathode tab is being cooled or not. As shown in Figure 6,

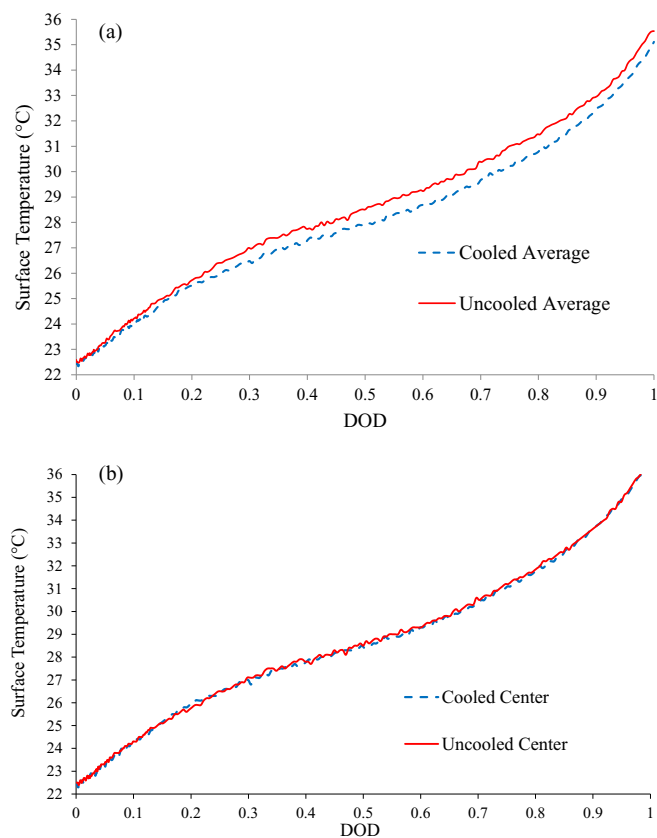


**Figure 6.** (a) Comparison of average surface temperature of the 14Ah cell for both the cooled and uncooled cathode tab stacks during 3C constant current discharge in natural convection. (b) Comparison of surface temperature at the center position of the cell face for both the cooled and uncooled cathode tab stacks during 3C constant current discharge in natural convection.

the average surface temperatures are closely alike between the cooled and uncooled cathode tabs during a 3C discharge. Therefore, this assumption holds reasonably well.

However, the same cannot be said for the 8C discharge. For the cell with an uncooled tab, the heat generation within the core should in fact become increasingly reduced as compared to its cooled tab counterpart. This is due to the increasingly higher temperature difference between the two as the discharge proceeds. Higher temperatures lead to better kinetics and, consequentially, lower heat generation. Therefore, the difference between the two heat curves in Figure 10 cannot be attributed solely to cathode tab heat. There is some unknown reduction of heat generation due to the improved kinetics and it has the

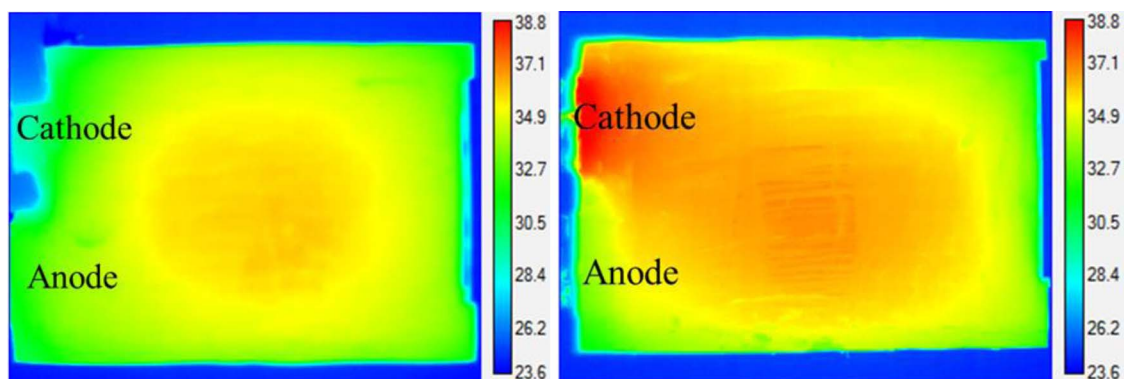


**Figure 7.** Infrared thermal images of cell at the end of a 3C discharge with a cooled cathode (left) and with no cooling on the cathode (right).

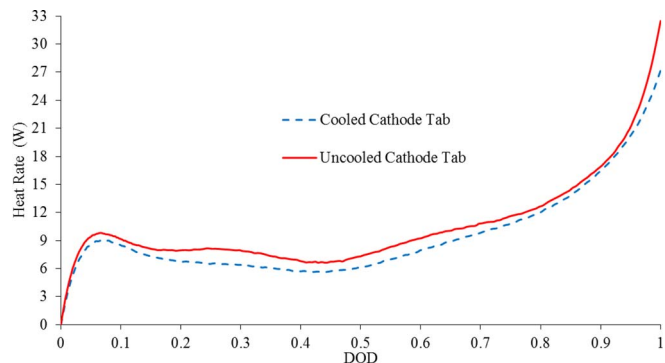


**Figure 8.** Comparison of heat rate calculated by LCM within the core of a 14Ah cell undergoing 3C constant current discharge.

effect of suppressing the true value of the cathode tab heat. A larger cathode tab heat value for the 8C discharge is directionally correct as it would tend to reduce the 10% gap between the theoretical ratio and the empirical ratio.

*Comparison of temperature gradients.*— Comparing average surface temperatures of each cell tells an incomplete story. Temperature gradients are also important. A cell that has an evenly distributed temperature (no gradients) has a chemical reaction rate proceeding evenly. However, a cell with sizeable temperature gradients has some areas of the cell core depleting prematurely and hampering performance. Even though two cells may have the same average surface temperature, the one with a greater temperature gradient is at a disadvantage. The effect that cooling the cathode tab has on thermal gradients is now investigated.

For each test run, the point at which the cell exhibited its maximum temperature gradient was identified. These thermal images were then compared to each other. The FLIR software has the capability to quantify the standard deviation of the temperature gradient over the surface. Analyses shows that for 99.7% (three standard deviations of an assumed normal distribution) of the cell surface, the highest temperature gradient during a 3C discharge was  $(3 \times 1.22^\circ\text{C}) = 3.66^\circ\text{C}$  with a cooled cathode. For an uncooled cathode grid tab at the same C-rate, it is  $(3 \times 1.05^\circ\text{C}) = 3.15^\circ\text{C}$ . The removal of cathode grid tab heat actually induces a slightly higher temperature gradient across the cell surface at a low C-rate discharge. The benefit of reducing temperature gradients by cooling the cathode tab stack is only slight. At an 8C discharge, the cell surface has merely  $0.76^\circ\text{C}$  less of a temperature gradient when the cathode tab is cooled. The results are summarized in Table II.

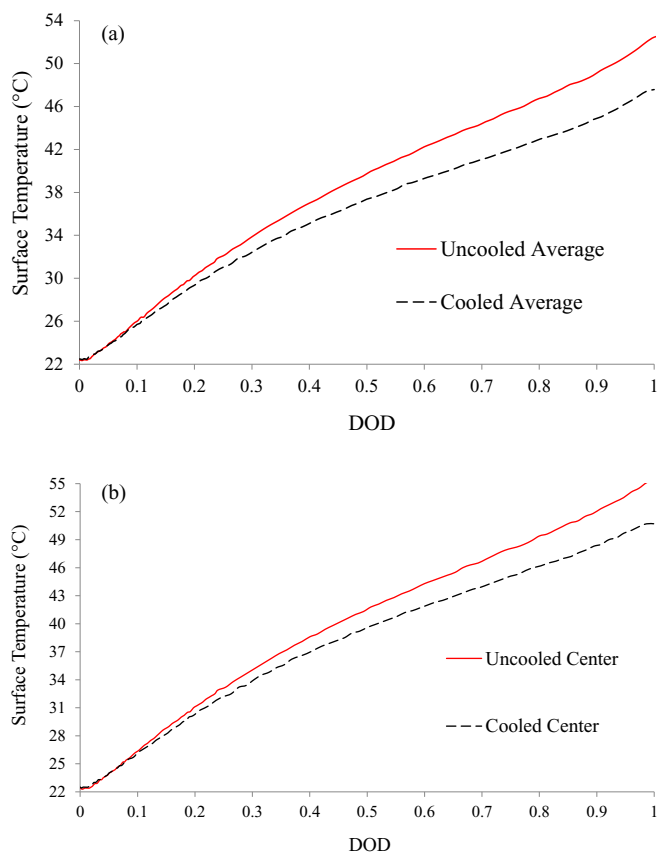


**Figure 9.** (a) Effect on the average surface temperature of cathode tab heat during 8C discharge of 14Ah cell in natural convection. (b) Effect on temperature of the cell face center due to cathode tab heat during 8C discharge of 14Ah cell in natural convection.

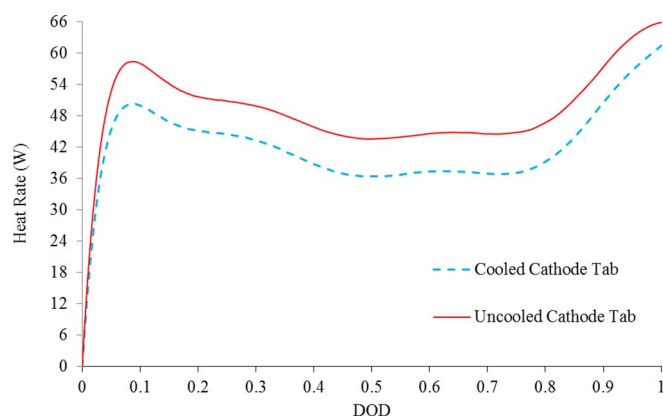


**Figure 10.** Comparison of heat rate within the cell with and without cooling of the cathode tab stack during 8C discharge. The 14Ah cell is initially at room temperature.

**Table II. Comparison of temperature gradients across cell surface at different rates of discharge as well as with and without cooling of the cathode grid tab stack.**

Rate of Discharge	Standard Deviation of Temp Gradient (°C)	
	Cooled Cathode	Uncooled Cathode
3C	1.22	1.05
8C	2.43	2.67

## Conclusions

Temperature and temperature uniformity both significantly affect the performance and life of energy storage devices and vehicles. This research investigated the feasibility of directly removing the heat generated at the tab joint of the cathode grids. The cathode was chosen to be studied since it generates significantly more heat than the anode. For this study, the use of a convection coefficient value derived from a lumped capacitance model was avoided because it was assumed to remain constant throughout the transient process. Instead, values derived from analytical equations in thermal boundary layer theory were used. This allowed a unique  $h$  value to be calculated for each temperature data point and yielded truer results.

The benefit to cell performance of removing the cell grid tab stack heat is not realized during low rates of discharge. During a constant current 3C discharge rate, heat from the cathode grid tab stack does not have the driving force to influence the temperature at the center of the cell throughout the cycle. Also, at 3C discharge, removing the cathode tab stack heat actually results in the increase of temperature gradients on the cell surface. It appears that the proximity of this heat source works in conjunction with the heat of electrochemical reaction in the cell core to minimize thermal gradients.

During an 8C discharge, the cathode tab heat begins to appear at the center of the cell face at 11% DOD. At this point, the combining of thermal loads attenuates the temperature gradients on the cell surface. Although cooling the cathode grid tab stack lowers the overall cell temperature by approximately 5°C, it has minimal benefit in reducing the statistical temperature gradient on the cell surface itself. Anode grid tab stack temperatures do not appreciably rise more than what is observed within the cell mass and does not warrant any cooling.

It should be noted that this temperature difference will also induce the cell core to generate less heat due to improved kinetics by some unknown amount. Care must be taken when making comparisons between the cooled and uncooled test runs and attributing any difference solely to the cathode tab heat. Quantifying this effect would require calorimetric testing.

## Acknowledgments

This research was supported by the Michigan Space Grant Consortium (MSGC). The MSGC creates, develops, and promotes programs that reflect NASA strategic interests in space-related science and technology in Michigan.

## References

1. R. Tamamushi, *Electrochemistry*, second ed., Maruzen, Tokyo, 2001.
2. K. Takano et al., *Journal of Applied Electrochemistry*, **32**, 251, 2002.
3. C.G. Motloch, J.P. Christopheresen, J.R. Belt, R.B. Wright, G.L. Hunt, R.A. Sutula, T. Duong, T.J. Tartamella, H.J. Haskins, and T.J. Miller, *High-Power Battery Testing Procedures and Analytical Methodologies for HEV's*, SAE 2002-01-1950.
4. E. V. Thomas, H. L. Case, D. H. Doughty, R. G. Jungst, G. Nagasubramanian, and E. P. Roth, *J. Power Sources*, **124**, 254 (2003).
5. M. Broussely, *Advances in Lithium-Ion Batteries*, W. A. V. Schalkwijk and B. Scrosati, editors, p. 393, Kluwer Academic/Plenum Publishers, New York (2002).
6. P. Arora, R. E. White, and M. Doyle, *J. Electrochem. Soc.*, **145**, 3647 (1998).
7. D. Aurbach, B. Markovsky, G. Salitra, E. Markevich, Y. Talyossef, M. Koltypin, L. Nazar, B. Ellis, and D. Kovacheva, *J. Power Sources*, **165**, 491 (2007).
8. M. Broussely, P. Biensan, F. Bonhomme, P. Blanchard, S. Herreyre, K. Nechev, and R. J. Staniewicz, *J. Power Sources*, **146**, 90 (2005).
9. J. Vetter, P. Novák, M. R. Wagner, C. Veit, K. C. Möller, J. O. Besenhard, M. Winter, M. Wohlfahrt-Mehrens, C. Vogler, and A. Hammouche, *J. Power Sources*, **147**, 269 (2005).
10. T. Huria, M. Ceraolo, J. Gazzarri, and R. Jackey, "Simplified Extended Kalman Filter Observer for SOC Estimation of Commercial Power-Oriented LFP Lithium Battery Cells", SAE International, 2013-01-1544, (2013).
11. S. Lee, T. Hyung Kim, S. Hu, Wayne W. Jeffrey, A. Abell, and J. Li, *J. Manuf. Sci. Eng.*, **135**(2), (2013).
12. M. Matheny, "Ultrasonic Metal Welding Foils to Tabs for Lithium-Ion Battery Cells", Cooperative Research Program, Summary Report SR-1301, August 2012.
13. R. Sabbah, R. Kizilel, J.R. Selman, and S. Al-Hallaj, S., *J. Power Sources*, **182**(2), 630 (2008).
14. S. Al Hallaj, H. Maleki, J. Hong, and J. Selman, *J. Electrochem. Soc.*, **83**, 98 (1999).
15. ASTM International, "Standard Practice for Infrared Thermography of Composite Panels and Repair Patches Used in Aerospace Applications", Designation E 2582-07.

16. D. Ibitayo, *Infrared Imaging of Power Electronic Components*, Army Research Laboratory ARL-TR-3690, December 2005.
17. T. M. Bandhauer, S. Garimella, and T. F. Fuller, *J. Electrochem. Soc.*, **158**(3) R1 (2011).
18. J. S. Hong, H. Maleki, S. A. Hallaj, L. Redey, and J. R. Selman, *J. Electrochem. Soc.*, **145**, 1489 (1998).
19. J. R. Incropera, J. R. DeWitt, J. R. Bergman, and J. R. Lavine, *Introduction to Heat Transfer*, Wiley, Fifth Edition (April 7, 2006).
20. <http://www.psychrometric-calculator.com/default.aspx#U9Mw0Tog99A>.
21. Formulations for the thermodynamic properties of the saturated phases of H<sub>2</sub>O from 173.15 K to 473.15 K, W. Hyland and A. Wexler, *ASHRAE Transactions*, **89**(2A) 500, 1983.
22. Formulations for the thermodynamic properties of dry air from 173.15 K to 473.15 K, and of saturated moist air from 173.15 K to 372.15 K, at pressures to 5 MPa, R. W. Hyland and A. Wexler, *ASHRAE Transactions*, **89**(2A) 520, 1983.